AIAA JOURNAL
Vol. 45, No. 9, September 2007

Coherent Structure Eduction and Convection Velocity in Compressible Blunt-Body Wakes

Alan L. Kastengren*
Argonne National Laboratory, Argonne, Illinois 60439
J. Craig Dutton†
University of Texas at Arlington, Arlington, Texas 76019
and
Gregory S. Elliott‡
University of Illinois at Urbana–Champaign, Urbana, Illinois 61801

DOI: 10.2514/1.29221

An iterative eduction procedure has been developed to study coherent structures in blunt-base cylinder wakes at 0 and 10 deg angles of attack to an $M = 2.46$ freestream flow. The eduction procedure uses an initial wavelet pattern to find candidate coherent structures of a particular scale and then uses the average intensity pattern of the educed structures to create an updated pattern. This iterative procedure continues until the average structure converges, indicating that a self-consistent intensity pattern has been described. Using this eduction procedure, the average appearance of the structures is described. Moreover, a convection velocity measurement is made by directly tracking individual coherent structures, unlike conventional imaging-based convection velocity measurements, which are not conditioned on coherent structures. The evolutionary trends of the structures are also quantified. The coherent structure averages show many of the same trends found in more conventional autocorrelation analysis. For example, the structures are inclined toward the freestream flow direction, and the angle of this inclination is affected by the recompression and reattachment processes. Convection velocity measurements show that the convection velocity is dependent on the transverse position of the structure in the shear layer, particularly for small structures. Finally, the coherent structures evolve in such a way that they become poorly representative of the average coherent structure pattern within 5–15 μs after being first identified.

Introduction

ORGANIZED vortical motions, known as coherent turbulent structures, are an important aspect of turbulent shear layer behavior [1]. These structures represent the largest eddies in the turbulent energy cascade, and they help to initiate the shear layer mixing and entrainment processes. A number of recent studies have shown that the behavior of the coherent structures in compressible shear layers is much different than in incompressible shear layers [2,3]. For example, the coherent structures in compressible shear layers are typically less organized and more three dimensional in nature than coherent structures in incompressible shear layers.

The convection velocity of the coherent structures is a particularly important parameter that is directly tied to the entrainment rate of fluid into the shear layer [4]. The coherent structure convection velocity is typically measured by examining double-pulsed visualizations of the shear layer and using a time-of-flight argument [2,5,6]. The convection velocity of coherent structures in compressible shear layers differs from the isentropic convection velocity seen in incompressible shear layers. The general consensus in the literature is that the structures follow a stream-selection rule [2]. The structures convect faster than the isentropic convection velocity in shear layers bounding a supersonic high-speed stream and a subsonic low-speed stream, while the structures convect more slowly than the isentropic convection velocity when the fluid on both sides of the shear layer moves supersonically.

Received 8 December 2006; revision received 11 April 2007; accepted for publication 13 April 2007.

*Postdoctoral Researcher, Energy Systems Division.
†Professor and Chair, Mechanical and Aerospace Engineering Department.
‡Associate Professor, Department of Aerospace Engineering.

A concern with the previous convection velocity measurements is that although it is ostensibly the coherent structures that are tracked, none of the previously cited studies ensure that a coherent structure is actually present in the original template window that is used in the method. This raises the possibility that the convection velocity data for the coherent structures have been combined with convection velocity data for incoherent features of the flow.

To track the structures through the flow explicitly, the structures must first be identified. One difficulty is in simply defining a "coherent structure." Various authors have proposed different definitions. One of the most widely cited is that of Hussain [7]: "A coherent structure is a connected turbulent fluid mass with instantaneously phase-correlated vorticity over its spatial extent." Although vorticity seems to be a good choice of a fundamental variable by which to define coherent structures, measuring vorticity on an instantaneous basis over an area or volume of a flow can be quite difficult. Thus, authors performing flow visualizations that do not measure vorticity define a coherent structure, either explicitly or implicitly, as a phase-correlated pattern in their visualizations [2,5,8].

Given a definition of a coherent structure, a procedure must be developed to identify and describe such structures. Many techniques have been used for structure eduction, and this is an area of ongoing research. Hussain [7], as well as Hussain and Hayakawa [9], measured the vorticity in several flows using hot-wire anemometer (HWA) rakes. They also developed a procedure for identifying vortical motions in the HWA data, as well as combining and phase averaging the signals to describe the average coherent structure. Two-dimensional velocity vector data available from particle image velocimetry allow the identification of structures by patterns in velocity [10] or out-of-plane vorticity [10,11]. A pattern-recognition method was used by Giralt and Ferré [12] and Scarano et al. [10] to identify structures. This method correlates the velocity field to a user-defined prototype pattern. Giralt and Ferré [12] performed this analysis iteratively, with the pattern being updated to better reflect the average appearance of the coherent structures. Autocorrelation

analysis of flow visualizations has also been used by many researchers to determine the average size and shape of coherent structures [13–15] though this technique does not identify individual coherent structures. Wavelet analysis is another technique that has been used to find the average size of coherent structures [11] and their motion [16].

In incompressible shear layers, studies have found a number of typical processes by which coherent structures evolve as the flow progresses [1,17]. These include rollover of the structures as they convect downstream, pairing of two structures through rotation about a common axis and eventual merger, and tearing of structures into two smaller structures, which are later consumed by adjacent larger structures. Pairing, in particular, has been considered vital to the growth of a shear layer. In highly compressible shear layers, there is disagreement in the literature on the nature of the evolution of coherent structures. Some studies indicate that structures do not evolve significantly as they progress downstream [2,18]. Others find significant evolution of structures [13,19], though in highly compressible shear layers none find strong evidence of the pairing and tearing motions commonly seen in incompressible shear layers. Most of these previous studies are limited to only two time-correlated images, however. This limits the ability of these previous visualization studies to capture the evolution of coherent structures. Only recently have multi-image flow visualization techniques been used, specifically to study the shear layers in compressible jet flowfields [19].

The current work focuses on the coherent structures in the wakes of blunt-base cylinders at 0 and 10 deg angles of attack to a Mach 2.46 freestream. A conditional averaging technique will be demonstrated that can identify and average the individual coherent structures in the shear layers of the wakes in both side- and end-view images. The convection velocity of the coherent structures in side-view images is measured and compared with convection velocity data using more conventional techniques. The conditionally averaged structures will be compared to previous autocorrelation analysis of the structures.

Experimental Setup

The experiments analyzed in this work have been described in detail elsewhere [20,21]. Two front-supported afterbodies that are 63.5 mm in diameter were examined. One was a simple blunt-base cylinder at 0 deg angle of attack (i.e., with the cylinder axis parallel to the freestream flow). The other was a cylinder bent at 10 deg angle of attack, with a nominal length-to-diameter ratio of 1.5. The freestream Mach number in these experiments was 2.46. Important flowfield parameters for both wakes are listed in Table 1. A schematic of the flowfield for the 10 deg angle-of-attack case is given in Fig. 1.

To visualize these wakes, a Mie-scattering technique was used [3]. Liquid ethanol was introduced into the supply airstream upstream of the flow facility. This ethanol evaporated and thoroughly mixed with the supply air. As the flow was accelerated to supersonic speeds, the static temperature dropped significantly, and the ethanol vapor recondensed via a homogeneous nucleation process into a cloud of droplets approximately 50 nm in diameter [22]. The droplets evaporated in subsonic regions of the flow, marking the shear layer interface and the embedded coherent structures. A sheet of laser light 800 μm thick was scattered from these droplets, and the side-scattered light was imaged with a charge-coupled device (CCD) camera. By using a sheet of laser light, a thin cross section of the flow could be imaged. The small diameter of the ethanol droplets ensured that the droplets accurately responded to temperature and velocity changes of the flow [23,24].

Table 1 Important flow parameters

α, deg	0	10
T_0, K	302 ± 2	303 ± 2
P_0, kPa	$545 \pm 3\%$	$510 \pm 3\%$
Re	56.4×10^6/m	52.6×10^6/m

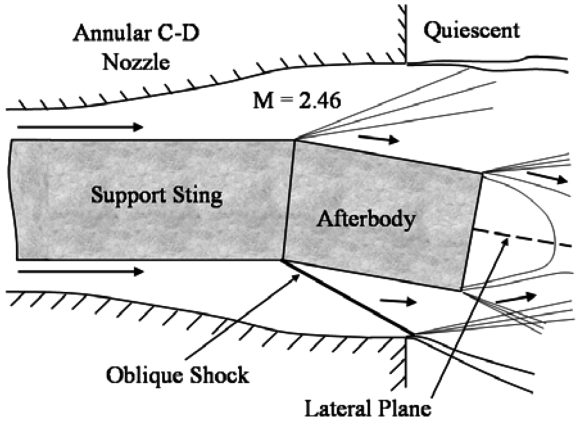

Fig. 1 Schematic of the angle-of-attack afterbody in the flow facility.

To examine the evolution of the coherent structures in detail, a multi-image flow visualization technique was used. The laser light source for this study was a pulse-burst laser, a relatively new type of laser capable of producing a short series of brief, intense laser pulses. For this study, the laser produced a series of 17 pulses approximately 20 ns each in duration (full-width half-maximum), with a time spacing between pulses of 2 μs. To capture the scattered light from this laser, a Dalsa 64K1M high-speed camera was used, which was capable of capturing time-correlated sequences of 17 images at rates of up to 1 MHz.

High-speed image sequences have been obtained at a number of locations in both the 0 and 10 angle-of-attack wakes, as shown in Fig. 2. For the axisymmetric wake ($\alpha = 0$ deg), side-view Mie-scattering visualizations have been obtained at four positions, roughly corresponding to positions B, C, D, and E of the single-shot imaging performed by Bourdon and Dutton [15]. These positions correspond to the developing shear layer, recompression, reattachment, and trailing wake regions, respectively. For the angle-of-attack wake ($\alpha = 10$ deg), side-view images were obtained for the windward symmetry plane (one position), leeward symmetry plane (one position), and lateral plane (three positions) shear layers.

For the axisymmetric wake, end-view images were obtained at locations corresponding approximately to the streamwise center of the side-view images. End-view images were obtained in the angle-of-attack wake at eight positions evenly spaced from 0.6 to 2.0R from the base surface, where $R = 31.75$ mm is the cylinder radius. A greater number of end-view imaging positions was deemed necessary in the angle-of-attack wake than in the axisymmetric wake to resolve the more complex three-dimensional evolution of the angle-of-attack wake near reattachment.

For all imaging positions, 650–800 sequences of 17 time-correlated images were obtained. Several image-processing steps were performed before the structure eduction analysis was undertaken. These steps are described in detail elsewhere [21–25]. First, the background was subtracted from the images, and images of large droplets were removed. Images were rejected in which there were too many bright or dark pixels, as were images for which the freestream seeding was insufficiently uniform. The freestream was also used to correct for the nonuniform intensity of the laser sheet. In addition, frequency-domain filtering was used in the end-view images to mitigate a regular banding pattern evident in the raw images. After processing, approximately 350–600 time-correlated image sequences at each location were deemed acceptable for further analysis.

Example Images

A few example image sequences from the high-speed visualizations will now be presented. A representative image sequence from the developing shear layer in the axisymmetric wake (position B in Fig. 2a) is given in Fig. 3. The flow is from left to right, with the freestream flow toward the top of the image and the

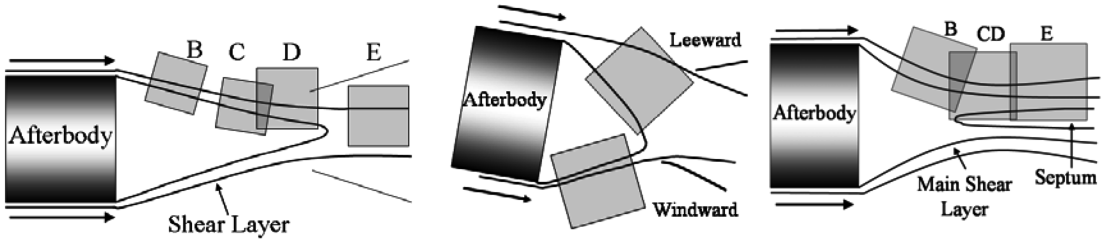

a) b) c)

Fig. 2 High-speed imaging positions, shown to scale. a) axisymmetric wake; b) symmetry plane, angle-of-attack wake; c) lateral plane, angle-of-attack wake.

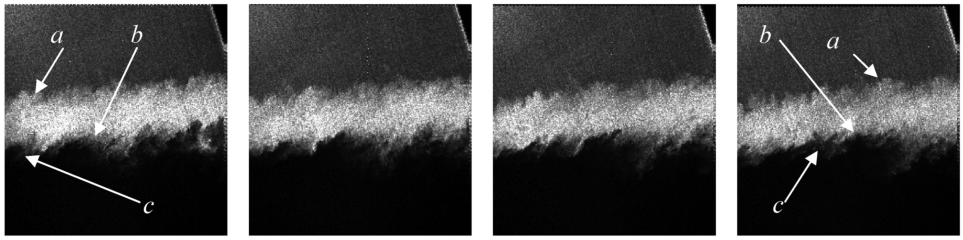

t = 0 t = 8 μs t = 16 μs t = 24 μs

Fig. 3 Sample side-view image sequence, position B ($x/R = 0.97$), axisymmetric wake; image height $0.80R$.

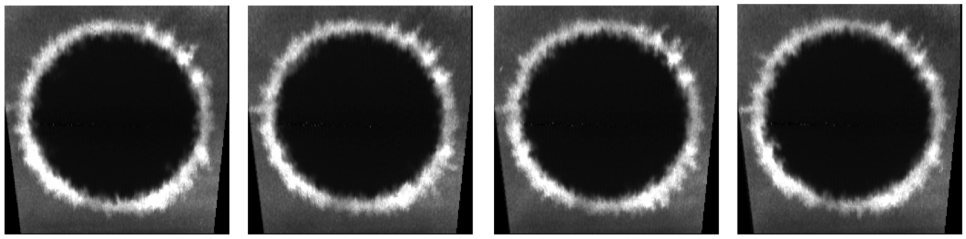

t = 0 t = 8 μs t = 16 μs t = 24 μs

Fig. 4 Sample end-view image sequence, position B ($x/R = 1.00$), axisymmetric wake; image height $2.28R$.

separated flow toward the bottom. A bright band of fluid is seen, which corresponds to the shear layer interface; the origin of this band is discussed in more detail in [25]. A series of small coherent structures is evident at the interface between the bright freestream fluid and dark recirculation region fluid. These structures can be tracked as the flow progresses, indicating a significant downstream convection velocity. The structures are also inclined toward the freestream flow direction and are quite disorganized, unlike the round, well-organized structures seen in incompressible shear layers. This image sequence demonstrates some of the challenges that must be overcome in describing the coherent structures in this flow.

End-view images provide further insights into the behavior of these flows. Figure 4 shows the behavior of the axisymmetric wake at end-view position B, in the free shear layer region. The mean freestream flow is directed out of the page. The structures here are relatively small and are on average symmetric in shape about a radial line through the structure's center.

Analysis Techniques

The high-speed image sequences are used to determine the convection velocity and evolution of the coherent structures. Before further analysis is undertaken, a working definition of coherent structure must be laid out. Upon examining the individual images, the coherent motions seem best defined as "intensity patterns in the image that occur over a significant region of the flow and that represent significant perturbations from the intensity pattern in the ensemble-average image." In light of this definition, before the convection velocity or structure eduction analyses are performed, the ensemble-average image is subtracted from the instantaneous images to remove the average intensity distribution from the images.

Side-View Images

Coherent Structure Eduction and Averaging

Although autocorrelation analysis of flow visualization images has been used in previous studies [13–15] to describe the coherent structures in supersonic shear layers, this technique is inherently statistical. It does not identify individual coherent structures and depends on a large ensemble of images to be successful. It would be preferable to describe coherent structures based on a technique that locates and averages the structures directly.

The current technique is based on an iterative eduction and averaging procedure conceptually similar to that used by Giralt and Ferré [12]. An idealized intensity pattern for the structures is assumed as an initial template pattern. This pattern is cross correlated with the first image of each visualization sequence. The position of maximum cross correlation is selected as the location of a candidate coherent structure (assuming the cross-correlation coefficient is above a fixed threshold). The intensity patterns of these structures are averaged,

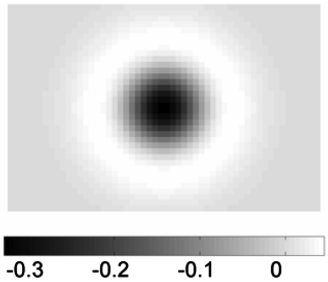

Fig. 5 Shape of initial Mexican hat template pattern to scale with the size of the template frame.

yielding an average intensity pattern similar, but not identical, to the initially assumed pattern. At this point, the "average" structure depends highly on the initially assumed pattern. To reduce this biasing effect, the procedure is performed iteratively. The average structure now becomes the new template pattern, and the procedure is repeated until the average converges. The final pattern is, in a sense, a conditional average of the intensity patterns in the images, showing a self-consistent intensity pattern across the image ensemble. The average pattern is deemed to have converged if the mean difference between it and the pattern of the previous iteration is less than 10% of the standard deviation of the pixel intensities in the frame. In preliminary tests, this convergence threshold provided generally good convergence of the average structure pattern within a reasonable number of iterations (usually 5–10). This becomes the definition of coherent structure in this study.

A potential pitfall with this structure eduction method is that when a small template is cross correlated with a larger image region, high correlation might result from a match between the edge of the template and a sharp gradient in the flow, rather than a match between the overall pattern in the template and large-scale structures in the images. To prevent this, a windowing filter is applied to the template, smoothing the intensity to zero near the edges of the frame. In a certain sense, the template pattern is transformed into a wavelet, in that it has a limited spatial extent and is smooth (i.e., it has compact support in the frequency domain).

The initially assumed pattern is an inverted Mexican hat wavelet. This pattern is isotropic, so that the initial pattern will not bias the shape of the final average structure pattern. The authors also investigated several other wavelet shapes in initial studies, but found the Mexican hat to be the most effective at educing coherent structures. The equation of the inverted Mexican hat wavelet is

$$\psi(x, y; a) = \left(\frac{x^2 + y^2}{a^2} - 2\right) \frac{1}{a} e^{\left(-\frac{x^2+y^2}{2a^2}\right)} \tag{1}$$

Here, the quantity a is the scale of the wavelet, which gives a measure of the width of the pattern. For this analysis, four wavelet scales are used: $a = \delta/16$, $\delta/8$, $3\delta/16$, and $\delta/4$, where δ is the shear layer thickness as determined from the Mie-scattering images. The frame around each wavelet is drawn to be $6a$ in height and $9a$ in width. This frame size was selected so that the Mexican hat wavelet is nearly zero at the edges of the frame, but nonzero for a significant portion of the middle of the frame. The shape of the initial template pattern and the template frame are shown in Fig. 5. These wavelet scales were used because the spatial resolution of the images was insufficient to investigate significantly smaller scales, and attempts to use larger scales simply did not provide a good fit to the typical coherent structures present in the images.

To demonstrate that this technique indeed identifies coherent structures, examples of the educed structures are given in Fig. 6. The ensemble average has been subtracted from these images, which accentuates both the coherent structures and the noise in the images. The boxes indicate the position and size of the frame that encloses the coherent structure that has been educed. The boxes clearly enclose at least a substantial part of well-defined coherent structures. These results are representative of the overall performance of the eduction scheme.

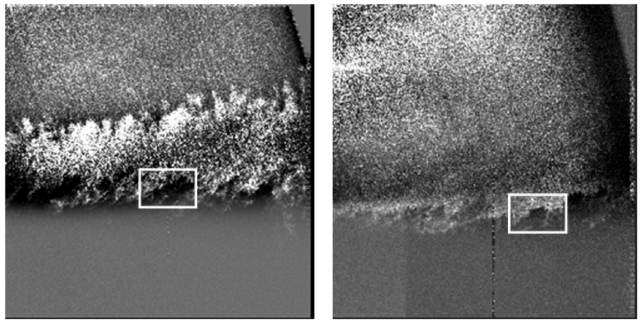

a) **b)**

Fig. 6 Examples of educed structures: a) axisymmetric shear layer, position B; b) angle-of-attack wake, windward shear layer.

There are some limitations to the structure eduction procedure. The procedure finds a single self-consistent image intensity pattern for each structure scale. If there are multiple types of coherent structures with different representative image intensity patterns, only one of these patterns will be detected. Also, the instantaneous views of the coherent structures are often quite disorganized. The individual coherent structures may not necessarily correlate well to this smooth average structure pattern, and some coherent structures may be missed. This is not of great concern given the large number of images and structures available at each imaging position; well-converged averages can still be obtained.

Cross-Correlation Technique

The structure eduction and convection velocity measurements in this paper are based on a cross-correlation technique. This technique is commonly used in the literature to find the region of an image where a template is best matched. By using part of the initial image of a time-correlated visualization as a template and using a time-of-flight argument, this technique allows convection velocity measurements to be made. The cross correlation is typically computed by a direct method, based on the equations given by Smith and Dutton [26] and Bendat and Piersol [27]:

$$\tilde{I}_n(x, y, t) = I(x, y, t) - \frac{1}{N} \sum_{n=1}^{N} I_n(x, y, t) \tag{2}$$

$$I'_n(r, s, \Delta x, \Delta y, t) = \tilde{I}_n\left(x_o + \Delta x - \frac{p}{2} + r, y_o + \Delta y - \frac{q}{2} + s, t\right) - \frac{1}{pq} \sum_{r=0}^{p-1} \sum_{s=0}^{q-1} \tilde{I}_n\left(x_o + \Delta x - \frac{p}{2} + r, y_o + \Delta y - \frac{q}{2} + s, t\right) \tag{3}$$

$$C_n(\Delta x, \Delta y, \tau) = \frac{\sum_{r=0}^{p-1} \sum_{s=0}^{q-1} I'_n(r, s, \Delta x, \Delta y, t + \tau) * I'_n(r, s, 0, 0, t)}{\sqrt{\sum_{r=0}^{p-1} \sum_{s=0}^{q-1} (I'_n(r, s, \Delta x, \Delta y, t + \tau))^2 * (I'_n(r, s, 0, 0, t))^2}} \tag{4}$$

The correlation window is p columns in width and q rows in height. The original template window is centered at (x_0, y_0), while the cross-correlation results are obtained for various points displaced $(\Delta x, \Delta y)$ in the subsequent images. $I_n(x, y, t)$ is the instantaneous intensity of point (x, y) in image n of the ensemble at time t. $\tilde{I}(x, y, t)$ is the deviation of the intensity at point (x, y) from the ensemble-average value for the pixel at time t. $I'(r, s, \Delta x, \Delta y, t)$ is the difference between $\tilde{I}(x, y, t)$ and the mean value over the template window at point (r, s) in the template window when the template

window is displaced $(\Delta x, \Delta y)$. $C_n(\Delta x, \Delta y, \tau)$ is the cross-correlation coefficient at displacement $(\Delta x, \Delta y)$ for a time delay of τ.

Although the direct cross-correlation technique is effective when correlating the template region over a small range of displacements (as is often done in convection velocity measurements), it is excessively intensive computationally for the structure eduction method. The cross correlation can be performed far more quickly using an fast Fourier transform (FFT) technique [27]. The FFT technique, however, requires calculation of the average and standard deviation of the image in the region where the template overlaps the image for every position of the template. To do this, both the image and the square of the image (i.e., each pixel intensity value squared) are convolved with a top-hat filter of the same size as the template. The resulting images represent the local average and sum of squares, respectively, of the regions where the template and image would overlap at every possible position of the template. From these data, the local standard deviation can be easily determined. The FFT technique is effective and far faster than the direct cross-correlation technique for the template sizes used in this work.

Conditioned Convection Velocity Measurements

The standard cross-correlation techniques used in previous studies are able to find the convection velocity of a region of fluid in time-correlated images. However, in most studies, no attempt is made to ensure that a large-scale structure is actually present in the area being tracked; these measurements are termed "unconditioned" in this work, because they are not explicitly conditioned on the presence of a coherent structure. In this study, the cross correlation has been performed when conditioned on the presence of coherent structures. The coherent structures are located through cross correlation with the average structure patterns described in the previous section. This instantaneous structure is then used as a template, and the position of the structure in later frames of the flow visualization is found by cross correlation. As in previous studies using multiframe visualizations [19], the structures are tracked across several frames of the visualization, with a linear fit performed between the successive displacement measurements and the time delay between the images to find the structure convection velocity. Because the average structures are educed at several scales, the conditioned convection velocity is computed separately for each of these scales. In this way, the convection velocity of the large-scale coherent structures can be compared to that of somewhat smaller-scale coherent structures. The tracking process is ended if the correlation coefficient between the template and the structure falls below 0.5 or if the structure reaches the edge of the image. Furthermore, velocity data are recorded only for those structures that can be tracked across at least three frames in the image sequence, because the velocity data contain a great deal of uncertainty if the structure is tracked across only two frames. Velocity measurements for which the relationship between position and time is not sufficiently linear are also rejected.

Coherent Structure Evolution

There has been far less quantitative study of the temporal evolution of coherent structures in compressible shear layers than of coherent structure convection velocity. Those studies that have been performed have largely been qualitative. This is in part because the coherent structures in highly compressible shear layers are generally disorganized in appearance, which makes it far more difficult to objectively classify the evolution of the structures.

In this study, two measures are used to quantify the evolution of the coherent structures. First, in previous unconditioned convection velocity measurements of these wakes, structures usually evolved relatively quickly as they moved downstream to such an extent that they no longer correlated well to their initial pattern [21]. Thus, the average time span over which structures can be tracked can be used as a measure of the time scale of the structure evolution.

The second measure quantifies the nature of the evolution of the structures. There are two possible ways in which a structure could evolve. First, the structure could dissipate and no longer be representative of the average coherent structures in the images. Second, the structure could morph so that it no longer correlates particularly well with the original shape of the structure, though it still correlates reasonably well to the average coherent structure pattern. To decipher which of these mechanisms is more important, the correlations of structures to both the initial realization of the structure and the average structure from the conditional averaging procedure are recorded. If the correlation of the structure to the average structure remains high as it evolves, this indicates that the structure remains representative of the typical coherent structures, indicating a morphing type of evolution. On the other hand, if the correlation of the structure to the average structure declines as it evolves, this indicates that the structure dissipates.

End-View Images

The same iterative coherent structure eduction and averaging routines used for the side-view images are employed to study the end-view images of the wake. Some modifications of the procedure are needed, however, for the end-view images. In the side-view images, the shear layer is nominally linear, so the orientation of the shear layer, and hence the coherent structures, with respect to the image is constant across each image. On the other hand, the wake is nominally circular in the axisymmetric and angle-of-attack wakes, and the orientation of the structure in the image depends on the area of the shear layer (i.e., windward, lateral, or leeward) in which the structure resides. To avoid such problems, the search for coherent structures is limited to a small region of the end-view images. The region across which the structures are identified is the same as the initial template region for previous unconditioned convection velocity measurements [21]. The region is 2δ in dimension transverse to the shear layer and 3δ in dimension along the shear layer. Within such a small region the shear layer remains more or less linear, allowing the same codes used to process the side-view images to be used. The region is centered along the shear layer at the same location as the centroid of the wake. Measurements were made on the left-hand side of the wake in the axisymmetric wake and in the main shear layer of the angle-of-attack wake, as well as in the septum. A diagram showing these locations is given in Fig. 7 for the angle-of-attack wake. In addition, the coherent structures were averaged and educed in the windward portion of the angle-of-attack wake before and including reattachment. Because of the poorer spatial resolution of the end-view images, results will be presented for only a single scale, with a frame dimension transverse to the shear layer of $3\delta/4$ (initial wavelet scale $a = \delta/8$).

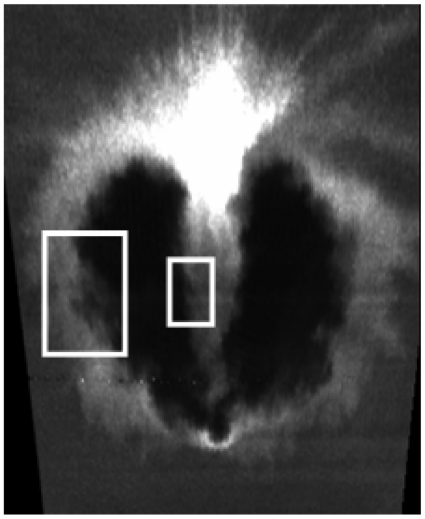

Fig. 7 Example image showing the positions for which structures are located and educed in the end-view images of the angle-of-attack wake.

Results

Side-View Images

Coherent Structure Averages

The coherent structures have been located and averaged at four scales for all of the side-view imaging positions. Figures 8–10 show the average structures for select imaging positions at three of these scales; see Fig. 2 for the definitions of the imaging positions. For all of these images, the flow is from left to right. For all images except Lateral CD Septum, the freestream is toward the top of the image; the "freestream" septum fluid is at the bottom of the Lateral CD Septum images. Several trends can be noted. First, the structures tend to consist of a roughly elliptical dark region, with a nearby region of particularly bright fluid, which is generally immediately above and upstream of the dark fluid. Although the structures look strikingly similar at most of the imaging locations, there are some important differences between them, especially at the smallest scale shown. In the axisymmetric wake, the angle of the interface between the bright and dark fluid seems more steeply inclined toward the freestream flow direction at positions C (not shown) and D than at positions B and E (not shown). This matches the structure angle trends observed in previous autocorrelation analysis of this wake [15]. In the symmetry plane of the angle-of-attack wake, the average structures in the windward shear layer look quite similar to those for the axisymmetric wake at small scales. However, the average structure in the windward shear layer is less regular at the larger scales. This matches the results of the autocorrelation analysis of this shear layer [20], which showed more irregular structures in the windward shear layer than in the axisymmetric wake [15] or the lateral plane of the angle-of-attack wake. The structures in the leeward part of the shear layer seem inclined at a high angle to the freestream flow direction. The appearance of these structures is unlike that of the structures at the other imaging positions, underlining the unusual behavior of the structures in the leeward shear layer described in previous work [20].

Figures 11 and 12 provide indications of the success of the conditional averaging technique. Figure 11 shows the mean correlation between the instantaneous and average structures at the various scales investigated. At the smallest scales, the mean correlation coefficient is generally between 0.7 and 0.8. Considering the irregular shape of the instantaneous structures, this shows that the average structure indeed represents the instantaneous structures quite well. As the scale increases, the mean correlation of the instantaneous structures to the average structure declines. This is not surprising, because limited imaging resolution and finite laser sheet thickness serve to smooth the images at the smaller scales more than at the larger scales, making the instantaneous structures resemble the smooth average structures better.

Figure 12 shows the average fraction of the images in which a structure of a particular scale could be located. The fraction is generally quite high (>70%) for the smallest scales. This fraction decreases as the scale increases for two reasons. First, structures are only added to the average if the frame around the structure lies completely within the image. As the scale of the structure (and hence the size of the frame) increases, less and less of the image is available to hold a valid structure. Second, a minimum level of correlation must exist between an intensity pattern in the image and the average structure before such a pattern is considered a valid coherent structure. Because the mean correlation between the instantaneous structures and the average structure declines as the scale increases, it seems reasonable that fewer structures would be accepted as the structure scale increases.

There are a few notable exceptions to these trends. The first is position B in the axisymmetric wake, where at the smallest scale the individual structures are both less well correlated to the average structure and are found less often than at the next largest scale. The reasons for this are not entirely clear. Other exceptions are the main and septum shear layers at position E in the lateral plane of the angle-of-attack wake. The shear layer at position E is quite disorganized. It seems that a single average intensity pattern simply cannot fully represent the coherent structures at this position.

Conditioned Convection Velocity Measurements

Figure 13 shows the conditioned convection velocity measurements for several imaging positions for the smallest coherent structure scale (frame height $h = 3\delta/8$). These data are displayed versus the transverse position of the educed structure in the shear layer. The zero point of the ordinate in these plots is the transverse location at 50% of the peak intensity in the ensemble-average image. The results are rather striking. There is a significant variation in convection velocity with transverse location in the shear layer for the axisymmetric shear layer at position B. Far above the shear layer interface, the convection velocity is quite uniform and near the velocity of the high-speed freestream (602 m/s) [28]. As one moves closer to the shear layer interface, the convection velocity decreases significantly. Although there is significant scatter in the data at any particular transverse position, there is a clear trend for the convection velocity to smoothly decrease as the transverse position in the shear layer decreases. Indeed, the pattern of the convection velocity variation with transverse position appears to be similar to the expected trend in the mean fluid velocity in the high-speed portion of a turbulent shear layer. The velocity measurements end below the shear layer interface, because the images are uniformly dark in this region, and no structures can be detected.

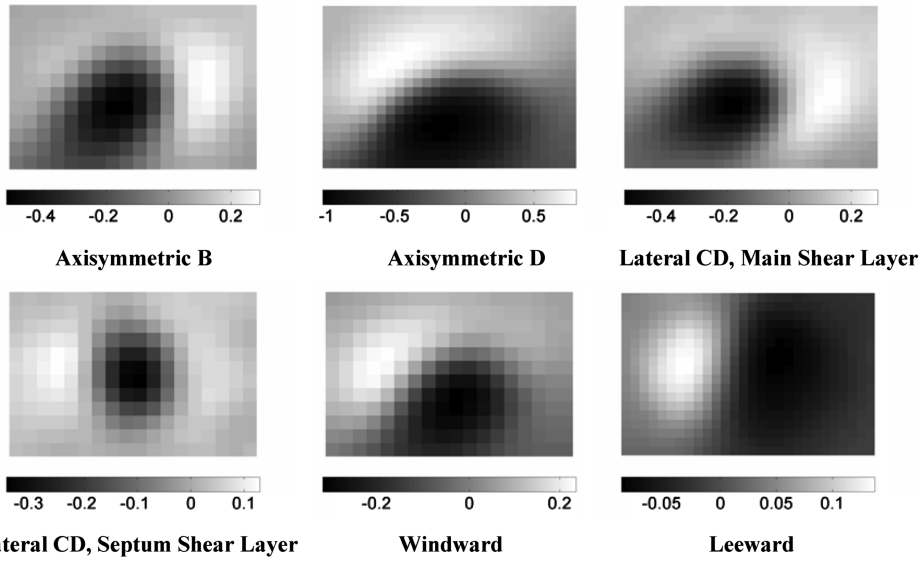

Fig. 8 Conditionally averaged structures for various side-view imaging positions. Frame height $h = 3\delta/8$. Scale is the average intensity of the structure normalized by the freestream intensity of the image.

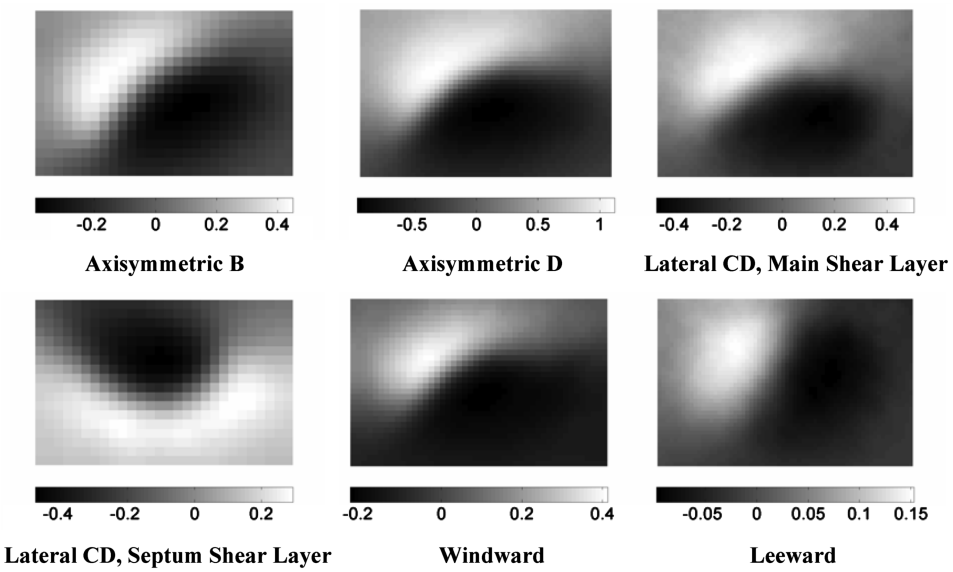

Fig. 9 Conditionally averaged structures for various side-view imaging positions. Frame height $h = 3\delta/4$.

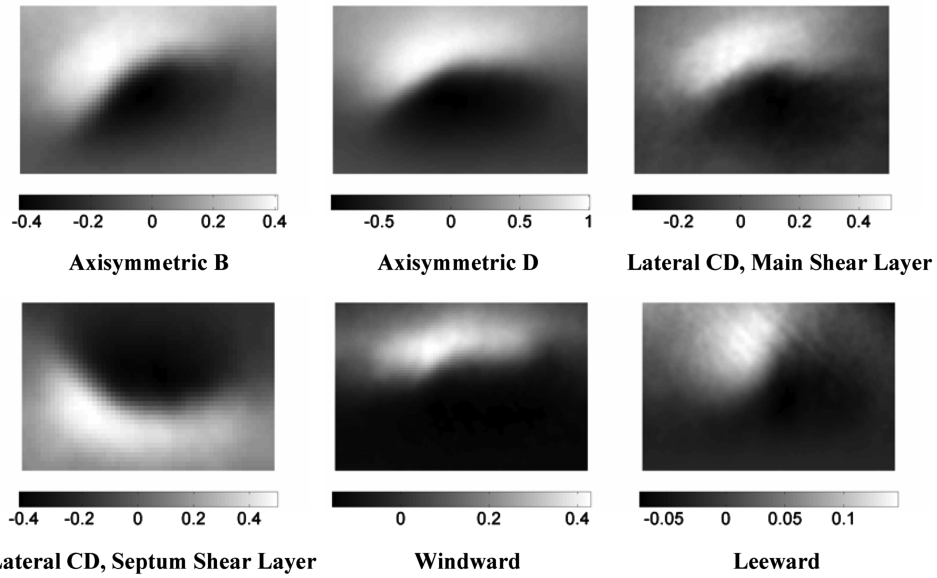

Fig. 10 Conditionally averaged structures for various side-view imaging positions. Frame height $h = 3\delta/2$.

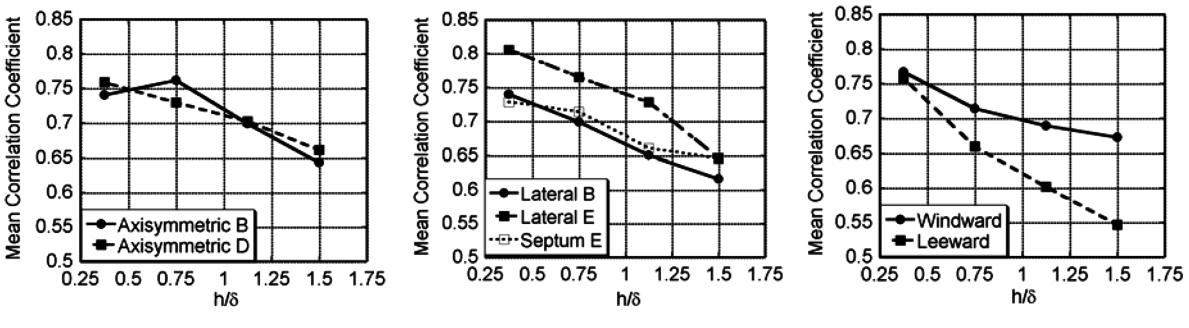

Fig. 11 Mean correlation between the average structure and the individual educed structures at four different scales for selected imaging positions: a) axisymmetric wake; b) lateral plane, angle-of-attack wake; c) symmetry plane, angle-of-attack wake.

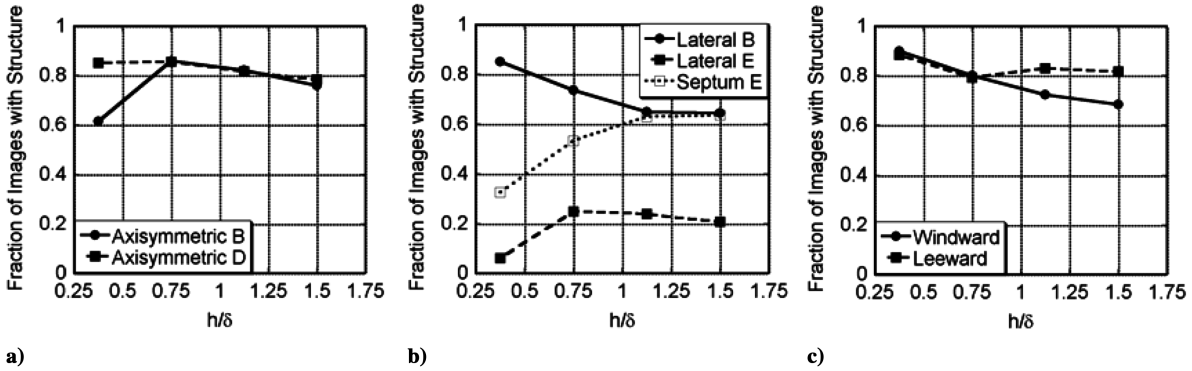

Fig. 12 Fraction of images in which the conditional averaging procedure located a structure at four different scales, for selected imaging positions: a) axisymmetric wake; b) lateral plane, angle-of-attack wake; c) symmetry plane, angle-of-attack wake.

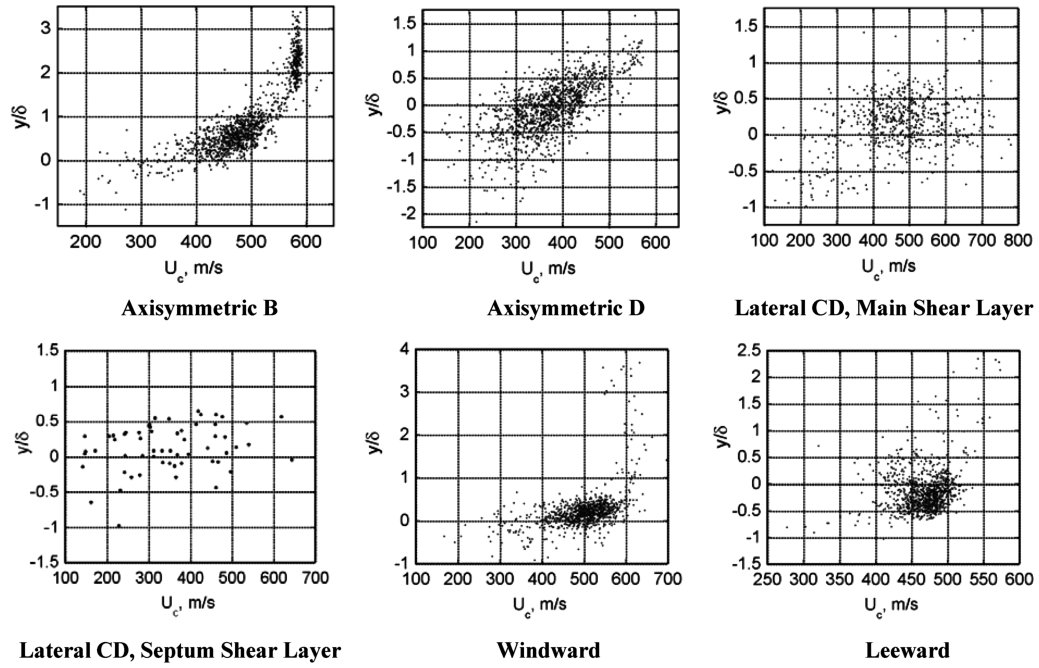

Fig. 13 Conditional convection velocity magnitude plotted vs transverse shear layer position for a structure frame height $h = 3\delta/8$.

For the remaining plots in Fig. 13, velocity realizations are only shown over a transverse range of approximately $-1.5 < y/\delta < 1.5$ for position D in the axisymmetric wake and the lateral plane of the angle-of-attack wake to allow comparisons to be made more easily between the results at different imaging positions. The distinct trend of decreasing convection velocity with decreasing transverse position is still clear at position D in the axisymmetric shear layer. There appears to be much more scatter in the velocity data at any given transverse location for this position than for position B. This is to be expected, because the motions of the coherent structures tend to become more disorganized in the reattachment region [15].

The results for the angle-of-attack wake are much more varied. For the lateral plane main and septum shear layers of the angle-of-attack wake, the scatter in the velocity measurements is much larger than for the axisymmetric wake at all of the imaging locations. Indeed, many measurements indicate convection velocities higher than the freestream velocity [28]. Although this result seems unrealistic, visual inspection of these realizations shows that these velocity measurements indeed match the apparent convection velocity of the structures in the images. This may be caused by a mean out-of-plane velocity component in this area of the wake indicated by previous unconditioned structure velocity measurements [21], which causes structures to rapidly appear and disappear in the images. Furthermore, the cross-correlation technique implicitly assumes that the fluid remains in the plane of the laser sheet as it convects downstream. The apparent convection velocity of structures may be misleading as they pass through the laser sheet, depending on their three-dimensional shape. Moreover, in the septum, there are far fewer valid velocity measurements, due to the rapid appearance and disappearance of structures in the visualizations [21].

For the windward shear layer, similar results to those seen in the axisymmetric shear layer are evident. This is consistent with the similarity in the appearance of this shear layer to the axisymmetric shear layer in the example high-speed images [21] and the similarity in the appearance of the average structures at these positions. The leeward shear layer results show that most of the velocity realizations are clumped in a narrow range of transverse locations, yielding a different distribution than that seen at the other imaging positions in these wakes. It is particularly interesting that most of the velocity realizations in the leeward shear layer are found at negative y locations, unlike what is seen in the axisymmetric wake or the windward shear layer. Given the peculiar behavior of the leeward shear layer documented previously [20], these unusual conditioned convection velocity results are not surprising.

To study the effect of the structure scale on convection velocity, Fig. 14 shows the convection velocity results for three scales for the

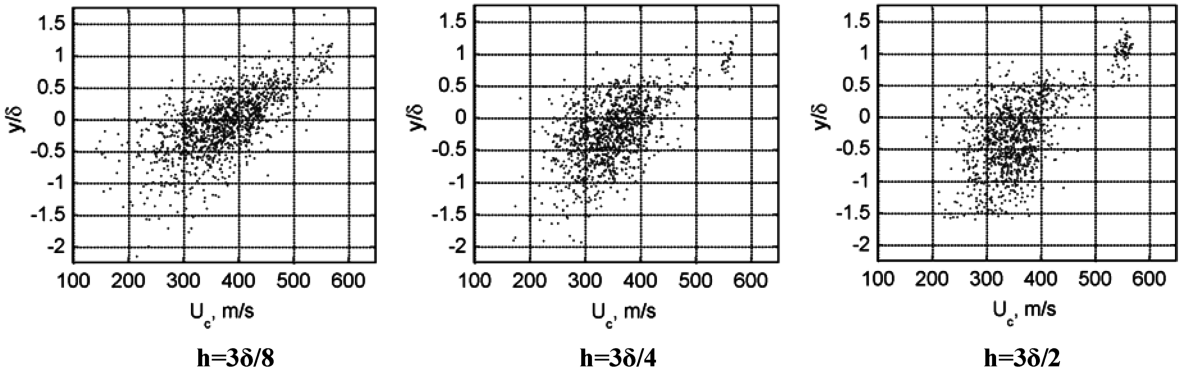

Fig. 14 Conditional convection velocity magnitude plotted vs transverse shear layer position for different structure scales in the axisymmetric wake shear layer at position D (reattachment).

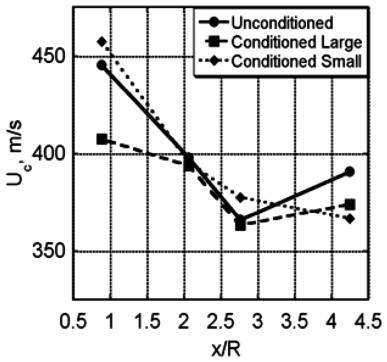

Fig. 15 Convection velocity for the axisymmetric wake as calculated by the unconditioned [21] and conditioned cross-correlation methods.

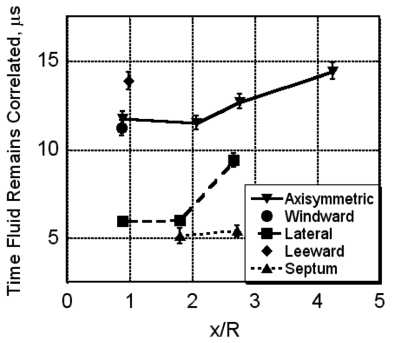

Fig. 16 Mean length of time over which the structures could be tracked in the conditioned convection velocity measurements at various imaging positions.

axisymmetric shear layer at position D. At all of the scales, there are a few structures at large transverse positions that convect at nearly the freestream velocity (602 m/s). Overall, as the scale of the structure increases, the variation in convection velocity with transverse position becomes less obvious. There are two possible causes for this. The largest scales could simply convect at a more nearly equal velocity at different transverse positions; this has been an assumption underlying previous unconditioned convection velocity measurements. This behavior may also be caused by smoothing due to the larger cross-correlation windows used as the size of the structure increases. These results are typical of the behavior seen at the other imaging positions examined in this study.

To make quantitative comparisons between the conditioned and unconditioned convection velocity measurements [21], the conditioned velocity data must be averaged in the transverse direction. Averaging has been performed across the region of the flow corresponding to the transverse extent of the template window in the unconditioned measurements, which corresponds roughly to the region from $y/\delta = -1.0$ to $y/\delta = 1.0$. This averaging has been performed both for the largest and the smallest scales, to demonstrate the different behavior of the different scales examined in this study.

The results of this analysis are shown in Fig. 15 for the axisymmetric wake. The uncertainty in these mean values is less than 6 m/s for all points plotted. There are differences between the convection velocity measurements for unconditioned cross-correlation analysis and for the two scales shown using the conditioned cross-correlation analysis, especially at position B ($x/R = 0.89$) and to a lesser extent at position E ($x/R = 4.25$). However, there does not appear to be a clear trend in these variations, and the conditioned convection velocity results follow roughly the same trend as the unconditioned velocity results. The convection velocity follows much different trends than the theoretical isentropic convection velocity. The reader is referred to [21] for a detailed comparison of the unconditioned convection velocity measurements, which follow the same trend as the current measurements, to the isentropic convection velocity.

Coherent Structure Evolution

The length of time for which a structure can typically be tracked in a visualization (i.e., the time period until the correlation coefficient with the original template pattern drops below 0.5) is shown in Fig. 16. These results are quite similar to corresponding data for unconditioned convection velocity measurements [21]. Although the correspondence between these results may not at first glance seem remarkable, the size of the frame used to encompass the coherent structures is much smaller for the conditioned convection velocity measurements than for the unconditioned measurements. Smith and Dutton [26] have shown that the success of unconditioned convection velocity measurements falls dramatically if small correlation windows are used. Thus, the ability of the conditioned convection velocity measurements to track a structure successfully over several frames using a small template window is strong evidence that the structure eduction procedure indeed selects intensity patterns that remain correlated over long periods of time, that is, coherent structures.

It is also interesting to note that the length of time for which the structures remain correlated is significantly longer for the symmetry plane in the angle-of-attack wake and for the axisymmetric wake than it is for the lateral plane main and septum shear layers in the angle-of-attack wake. This result matches the appearance of the example images [21] and is probably due to out-of-plane motion in the lateral plane.

In theory, the lifetime of the coherent structures could depend on the transverse position of the structure in the shear layer. For example, one might expect structures near the freestream would survive longer than structures near the recirculation region, due to the

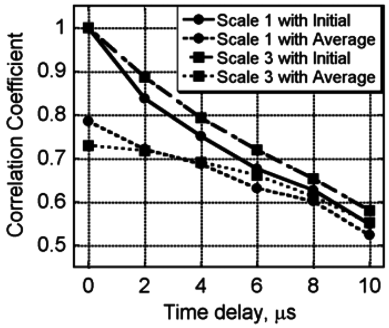

Fig. 17 Trend in the mean correlation of the coherent structures to the initial realization of the structure and to the average structure during conditioned convection velocity measurements at two scales ($h = 3\delta/8$ and $h = 9\delta/8$) for the axisymmetric wake at position B. Included are only those velocity measurements for which the structure could be tracked for six frames (10 μs).

lower level of shear near the freestream. Analysis of the data from the cross-correlation analysis, however, shows no such relationship.

Figure 17 shows the mean correlation of the structures both to the initial realization of the structure and to the average structure for the axisymmetric shear layer at position B at two different scales. The results are averages for structures that remained correlated for six frames, the mean number of frames over which a structure could be tracked in the visualizations. The correlation of the structure to the initial realization of the structure decreases as the time delay increases. This is expected, both from the previous high-speed visualization work of Thurow et al. [19] and from previous unconditioned convection velocity measurements [21]. There is no striking difference in the behavior of the different scales, suggesting that the structures at different scales evolve in a similar manner. More important, the correlation of the structure to the average structure also drops significantly as the flow progresses for both scales. Thus, it seems that as the coherent structures evolve, they tend to dissipate, rather than morph. These trends are typical, both for structures that can be tracked for different lengths of time at this position and for different imaging positions.

End-View Images

Overall, the success of the conditional averaging in the end-view images is comparable to the success of the routine in the side-view images. The conditionally averaged structures for the axisymmetric wake are presented in Fig. 18. In these images, the recirculation region is toward the right, with the flow out of the page, and the shear layer is nominally vertical (similar to the orientation of the left box in Fig. 7). Overall, the structures consistently show a region of dark fluid near the recirculation region (right-hand side of the image) bordered by bright fluid near the freestream (left-hand side of the image). The structures are well rounded and show a rather well-organized appearance. Although the structures in the axisymmetric wake are not entirely symmetric, as one would expect, there does not seem to be a definite pattern in the deviations from symmetry, and the asymmetry is in any case not substantial.

The appearance of the structures in the lateral region of the angle-of-attack wake is shown in Fig. 19, which is in the same orientation as the images in Fig. 18 (see Fig. 7). Perhaps the most striking feature of these structures is the inclination of the structures. Near separation ($x/R = 0.6$), the structures are strongly inclined toward the leeward side of the wake. This can quite clearly be tied to the inclination of the structures seen in previous autocorrelation analysis of this wake [20]. The inclination of the structures in the end-view images of the angle-of-attack wake appears to be the result of circumferential flow in the freestream around the wake, in the same manner as the coherent structures in side-view images tend to be inclined toward the freestream flow direction [20].

The trend in the inclination angle of the structures is also quite interesting. As the flow progresses downstream, the inclination becomes progressively smaller. There are two possible explanations

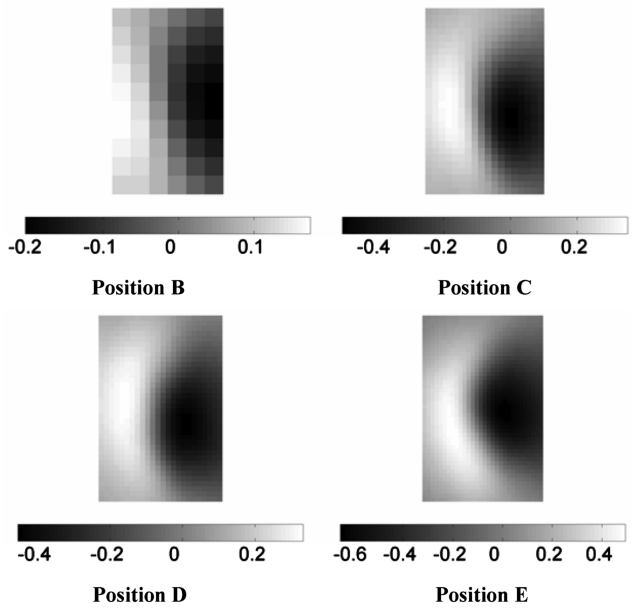

Fig. 18 Conditionally averaged structures, axisymmetric wake, frame width $h = 3\delta/4$. The scale of the shading in the images is the average intensity deviation from the ensemble average divided by the freestream intensity.

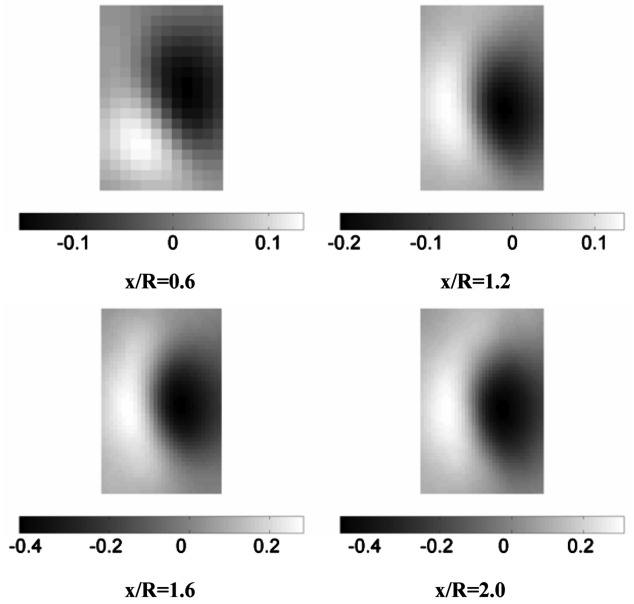

Fig. 19 Conditionally averaged structures, lateral region, angle-of-attack wake, $h = 3\delta/4$.

for this phenomenon. First, the structures are physically much larger and less well organized in appearance in the example images at more downstream locations in the wake, potentially blurring and obscuring the inclination of the average structure [20]. Another explanation is that the shear in the circumferential direction across the shear layer could be smaller at more downstream locations (i.e., a thicker shear layer), leading to less inclination of the coherent structures. It is possible that the strong circumferential flow around the angle-of-attack wake [21] induces a circumferential velocity throughout the wake core, reducing the circumferential shear across the shear layer.

The coherent structures have also been averaged in the septum shear layer of the angle-of-attack wake (see Fig. 7). The average structures in this region are displayed in Fig. 20. In these images, the

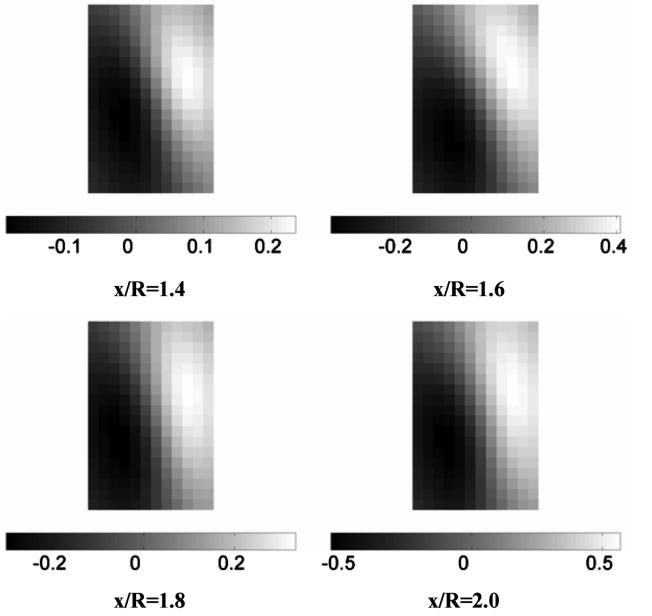

Fig. 20 Conditionally averaged structures, septum shear layer, angle-of-attack wake, $h = 3\delta/4$.

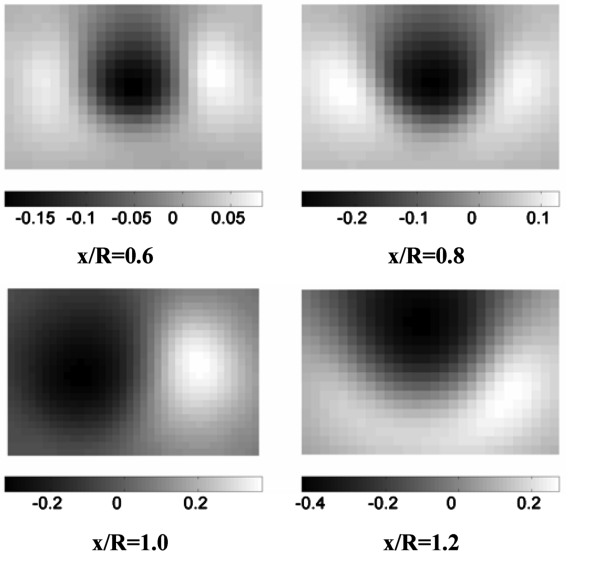

Fig. 21 Conditionally averaged structures, windward shear layer, angle-of-attack wake, $h = 3\delta/4$.

flow is again out of the page, with the shear layer nominally vertical and the recirculation region to the left. Unfortunately, the spatial resolution of these images is limited. It is apparent that the structures are associated with an inclined interface between the recirculation region and the bright region of the septum. The structures are inclined in the same direction as the flow in the bright region of the septum (i.e., downward in the images), which is consistent with the circumferential convection velocity of the structures in the septum shown in previous work [21].

Finally, the average coherent structures in the windward shear layer region of the angle-of-attack wake are shown in Fig. 21 upstream of and including reattachment ($x/R = 0.6$–1.2). To orient the reader, the freestream is toward the bottom of the image, with the recirculation region toward the top. For the first two imaging positions, the most striking feature of the images is how well organized the structures appear. The structures are relatively small compared to the size of the frame and quite symmetrical, with a central dark region surrounded by brighter fluid. The structures also appear to be wider near the recirculation region (top of the frames) than near the freestream (bottom of the frames). This is an interesting result. It is in stark contrast to the autocorrelation analysis of single-frame images for the axisymmetric wake, which indicated that the coherent structures were wedge shaped and were wider near the freestream than near the recirculation region [15]. However, the autocorrelation contours for the windward shear layer showed structures that were wider near the recirculation region than near the freestream, much like is seen here [20]. At mean reattachment ($x/R = 1.2$), the structures are also reasonably symmetric, though not so much as at the most upstream positions.

The shape of the structures is much different for $x/R = 1.0$, which presents an interesting case. As the averaging procedure converged for this position, the average structure pattern initially converged toward a pattern similar to the other windward average structure patterns. However, the routine eventually converged to the pattern shown in Fig. 21. The authors do not believe that the coherent structures are shaped significantly different at $x/R = 1.0$ than at the other imaging positions shown in Fig. 21. Indeed, conditional averaging with a smaller ($h = 3\delta/8$) and a larger ($h = 9\delta/8$) initial wavelet scale converged to shapes similar to the average structures for the windward shear layer at other imaging positions. The authors believe that the conditional averaging, in fact, is focusing at this position on the right-hand side of larger coherent structures shaped like those in the windward shear layer at other streamwise positions, yielding a nearly vertical interface between the bright and dark regions of the image.

This phenomenon demonstrates a limitation of the conditional averaging procedure. The procedure finds self-consistent intensity patterns in the visualizations. If there are multiple such self-consistent intensity patterns in a set of images, the pattern to which the procedure eventually converges depends on the choice of the initial template pattern, the character of the individual images in the image ensemble, and the convergence threshold used in the conditional averaging. Thus, it is best to interpret trends in these results by examining the results at a series of imaging positions. Although individual imaging positions may give misleading results, the trends become clear when viewing the average structures from multiple locations.

Moreover, this phenomenon brings into focus the question of the role of the structure scale. The structure scale discussed in this work is the scale of the initial wavelet pattern. As the averaging procedure progresses, the pattern is free to grow and shrink, to some extent. The windowing filter used to smooth the edges of the template pattern should act to restrain this change in size. However, it should be borne in mind that the size of the conditionally averaged structure may not correspond to the size of the original template pattern used, especially if structures of a different scale dominate the shear layer behavior.

Discussion

One of the most important conclusions of this work is on the nature of the convection velocity of coherent structures. Most previous studies have assumed that the coherent structures convect at a single, well-defined convection velocity at a given streamwise location [2,5,18,19]. However, the current conditioned convection velocity results show clear evidence that the convection velocity of the coherent structures in these wakes is highly dependent on the transverse position of these structures in the shear layer. This is in agreement with the conclusions of studies by Elliott et al. [29] and Murray and Elliott [30], which are two of the few previous studies that specifically examined the variation in convection velocity with transverse position in compressible shear layers.

This conclusion has significant implications for the interpretation and use of the stream-selection rule in describing coherent structure convection. The Mie-scattering method used to image the coherent structures in this study only shows fluid that moves supersonically with respect to the base flow model. Thus, the low-speed side of the shear layer and any structures residing in it cannot be imaged. If the coherent structures were consistently large and always resided at nearly the same transverse position in the shear layer, unconditioned convection velocity measurements obtained from these visual-

izations might still provide a good estimate of the average convection velocity of the coherent structures. However, the conditioned convection velocity measurements and the appearance of the conditionally averaged structures show that neither of these assumptions is valid. It seems inevitable that unconditioned convection velocity measurements in these Mie-scattering visualizations will be biased toward high velocity values, because the convection velocity of the structures is measured only in the higher-speed portion of the shear layer.

Mie-scattering techniques have been used in many of the previous studies of convection velocity in compressible shear layers, especially for shear layers between a supersonic high-speed stream and a subsonic low-speed stream [19,26]. Because of this biasing, it would be expected in these studies that even if the coherent structures move at near the local fluid velocity and are uniformly distributed across the shear layer, the convection velocity measurements will show higher convection velocity values than the isentropic convection velocity, agreeing with the stream-selection rule. It seems prudent that the results of these previous studies be carefully scrutinized in light of these potential biasing effects.

These data also provide interesting insights on the evolution of the coherent structures. The rate at which these structures evolve is rather remarkable. For example, at position B of the axisymmetric wake, the structures remain correlated for only 10 μs on average. In addition, the plots tracking the correlation of a structure to both the initial view of the structure and the average structure demonstrate quantitatively that the structures can no longer be tracked after a certain period of time because they dissipate. This gives firm evidence that the coherent structures in the current supersonic wakes evolve significantly, contrary to the results of some previous studies [2,8].

The conditional averaging and convection velocity measurement techniques presented here have important advantages and disadvantages over the conventional unconditioned convection velocity measurement technique. Unconditioned convection velocity measurements are quite straightforward and have only a few adjustable parameters. As Fig. 14 shows, the unconditioned measurements can provide useful average convection velocity data; the average convection velocity found with the conditioned technique is similar to that found with the unconditioned technique. The current analysis, however, provides a wealth of data that the unconditioned measurements cannot. The conditioned measurements track only an individual structure, not a broad region of the fluid, so the velocity measurements will be subject to less inherent smoothing and averaging than the unconditioned convection velocity measurements. Thus, the conditioned data can better represent gradients in the convection velocity across the flow, such as the variation in convection velocity with transverse shear layer position described earlier. Also, because the conditioned convection velocity measurements track individual structures, the evolution of these structures can be studied quantitatively, which cannot be done with the unconditioned convection velocity measurements.

The results of the conditional averaging of the coherent structures are also quite important. This study has demonstrated that it is possible to educe the irregularly shaped and spaced coherent structures in highly compressible shear layers. This technique is applicable to other flowfields and imaging techniques, so long as the coherent structures are distinct in the images. Indeed, the disorganized nature of the structures in this study made eduction of the structures particularly challenging. The authors suspect that this technique may be even more successful in flowfields with better organized structures.

The coherent structure averages also show generally good agreement with the results of autocorrelation analysis of these wakes [15,20]. The autocorrelation analysis accurately deciphered the overall shape and inclination angle of the coherent structures. This confirms that autocorrelation analysis is indeed a valid tool for studying the shape of coherent structures in flow visualizations. This is a useful result, because autocorrelation analysis is much simpler to implement and involves far fewer calculations than the conditional averaging procedure described in this study. Moreover, it confirms the validity of the previous studies of coherent structures that have used autocorrelation analysis [13–15].

Conclusions

The coherent structures in two supersonic blunt-base cylinder wakes have been described using a new structure eduction technique. This technique uses an assumed template pattern and iteratively refines the template to identify structures. In this way, the technique effectively finds self-consistent intensity patterns in flow visualizations of these wakes. This eduction technique has been applied to multiframe flow visualizations to obtain coherent structure convection velocity measurements conditioned specifically on coherent structures, as well as quantitative measurements regarding structure evolution. The coherent structure averages in general show many of the same features as previous autocorrelation analysis of these wakes. The convection velocity was on average quite similar to that seen in previous unconditioned convection velocity measurements of these wakes. However, the conditional convection velocity measurements showed a significant gradient in convection velocity across the shear layer. Finally, the structure evolution appears to proceed in such a way that after a relatively short period of time, the structures tend to dissipate.

Acknowledgments

This work was supported by the U.S. Army Research Office, Grant No. DAAD19-01-1-0367, with Thomas Doligalski as technical monitor. We would also like to acknowledge support for the pulse-burst laser and high-speed camera as part of a Defense University Research Instrumentation Program (DURIP) grant from the U.S. Air Force Office of Scientific Research (AFOSR) (Grant No. F49620-02-1-0283) with John Schmisseur as technical monitor. The authors thank James Norby and Jim Zhu at Continuum Lasers for their work in constructing the pulse-burst laser used in this study. Also, we would like to thank Walter Lempert and Brian Thurow at The Ohio State University for their expertise and guidance in pulse-burst lasers.

References

[1] Brown, G., and Roshko, A., "On Density Effects and Large Structure in Turbulent Mixing Layers," *Journal of Fluid Mechanics*, Vol. 64, No. 4, 1974, pp. 775–816.

[2] Papamoschou, D., and Bunyajitradulya, A., "Evolution of Large Eddies in Compressible Shear Layers," *Physics of Fluids*, Vol. 9, No. 3, March 1997, pp. 756–765.

[3] Clemens, N. T., and Mungal, M. G., "Large-Scale Structure and Entrainment in the Supersonic Mixing Layer," *Journal of Fluid Mechanics*, Vol. 284, Feb. 1995, pp. 171–216.

[4] Dimotakis, P., "Two-Dimensional Shear-Layer Entrainment," *AIAA Journal*, Vol. 24, No. 11, Nov. 1986, pp. 1791–1796.

[5] Murakami, E., and Papamoschou, D., "Eddy Convection in Coaxial Supersonic Jets," *AIAA Journal*, Vol. 38, No. 4, April 2000, pp. 628–635.

[6] Poggie, J., and Smits, A., "Large-Scale Structures in a Compressible Mixing Layer over a Cavity," *AIAA Journal*, Vol. 41, No. 12, Dec. 2003, pp. 2410–2419.

[7] Hussain, A., "Coherent Structures and Turbulence," *Journal of Fluid Mechanics*, Vol. 173, Dec. 1986, pp. 303–356.

[8] Arnette, S., Samimy, M., and Elliott, G., "Structure of Supersonic Turbulent Boundary Layer After Expansion Regions," *AIAA Journal*, Vol. 33, No. 3, March 1995, pp. 430–438.

[9] Hussain, A., and Hayakawa, M., "Eduction of Large-Scale Organized Structures in a Turbulent Plane Wake," *Journal of Fluid Mechanics*, Vol. 180, July 1987, pp. 193–229.

[10] Scarano, F., Benocci, C., and Riethmuller, M., "Pattern Recognition Analysis of the Turbulent Flow Past a Backward Facing Step," *Physics of Fluids*, Vol. 11, No. 12, Dec. 1999, pp. 3808–3818.

[11] Schram, C., Rambaud, P., and Riethmuller, M., "Wavelet Based Eddy Structure Eduction from a Backward Facing Step Flow Investigated Using Particle Image Velocimetry," *Experiments in Fluids*, Vol. 36, No. 2, 2004, pp. 233–245.

[12] Giralt, F., and Ferré, J., "Structure and Flow Patterns in Turbulent Wakes," *Physics of Fluids A*, Vol. 5, No. 7, July 1993, pp. 1783–1789.

[13] Poggie, J., and Smits, A. J., "Large-Scale Coherent Turbulence Structures in a Compressible Mixing Layer Flow," AIAA Paper 96-0440, Jan. 1996.

[14] Smith, K. M., and Dutton, J. C., "Investigation of Large-Scale Structures in Supersonic Planar Base Flows," *AIAA Journal*, Vol. 34, No. 6, June 1996, pp. 1146–1152.

[15] Bourdon, C. J., and Dutton, J. C., "Planar Visualizations of Large-Scale Turbulent Structures in Axisymmetric Supersonic Separated Flows," *Physics of Fluids*, Vol. 11, No. 1, Jan. 1999, pp. 201–213.

[16] Schram, C., and Riethmuller, M., "Vortex Ring Evolution in an Impulsively Started Jet Using Digital Particle Image Velocimetry and Continuous Wavelet Analysis," *Measurement Science and Technology*, Vol. 12, No. 9, 2001, pp. 1413–1421.

[17] Winant, C., and Browand, F., "Vortex Pairing: The Mechanism of Turbulent Mixing-Layer Growth at Moderate Reynolds Number," *Journal of Fluid Mechanics*, Vol. 63, No. 2, 1974, pp. 237–255.

[18] Mahadevan, R., and Loth, E., "High-Speed Cinematography of Compressible Mixing Layers," *Experiments in Fluids*, Vol. 17, No. 3, 1994, pp. 179–189.

[19] Thurow, B., Samimy, M., and Lempert, W., "Compressibility Effects on Turbulence Structures of Axisymmetric Mixing Layers," *Physics of Fluids*, Vol. 15, No. 6, June 2003, pp. 1755–1765.

[20] Kastengren, A. L., and Dutton, J. C., "Large-Structure Topology in a Three-Dimensional Supersonic Base Flow," *AIAA Journal*, Vol. 43, No. 5, May 2005, pp. 1053–1063.

[21] Kastengren, A. L., Dutton, J. C., and Elliott, G. S., "Large-Scale Structure Visualization and Convection Velocity in Supersonic Blunt-Base Cylinder Wakes," *Physics of Fluids*, Vol. 19, No. 1, Jan. 2007, paper no. 015103.

[22] Clemens, N. T., and Mungal, M. G., "A Planar Mie Scattering Technique for Visualizing Supersonic Mixing Flows," *Experiments in Fluids*, Vol. 11, Nos. 2–3, 1991, pp. 175–185.

[23] Wegener, P., Clumpner, J., and Wu, B., "Homogeneous Nucleation and Growth of Ethanol Droplets in Supersonic Flow," *Physics of Fluids*, Vol. 15, No. 11, Nov. 1972, pp. 1869–1876.

[24] Samimy, M., and Lele, S., "Motion of Particles with Inertia in a Compressible Free Shear Layer," *Physics of Fluids A*, Vol. 3, No. 8, Aug. 1991, pp. 1915–1923.

[25] Kastengren, A. L., Time-Resolved Visualization and Analysis of Compressible Blunt-Base Cylinder Wakes, Ph.D. Dissertation, University of Illinois at Urbana–Champaign, Urbana, IL, 2005.

[26] Smith, K., and Dutton, J., "A Procedure for Turbulent Structure Convection Velocity Measurements Using Time-Correlated Images," *Experiments in Fluids*, Vol. 27, No. 3, 1999, pp. 244–250.

[27] Bendat, J., and Piersol, A., *Random Data Analysis and Measurement Procedures*, Wiley Interscience, New York, 2000.

[28] Boswell, B. A., and Dutton, J. C., "Velocity Measurements in a Three-Dimensional Compressible Base Flow," *AIAA Journal*, Vol. 41, No. 5, May 2003, pp. 785–794.

[29] Elliott, G., Samimy, M., and Arnette, S., "The Characteristics and Evolution of Large-Scale Structures in Compressible Mixing Layers," *Physics of Fluids*, Vol. 7, No. 4, April 1995, pp. 864–876.

[30] Murray, R., and Elliott, G., "Characteristics of the Compressible Shear Layer over a Cavity," *AIAA Journal*, Vol. 39, No. 5, May 2001, pp. 846–856.

F. Coton
Associate Editor